Motion Behavior of The Suction Caisson Induced by Adjacent Spudcan Penetration in Sand

Yukun Zhang[1], Dayong Li[1,2], Qian Xiang[1,*] and Senjie Tong[3]

[1]*School of Civil and Architectural Engineering, Shandong University of Science and Technology, Qingdao, China*

[2]*College of Pipeline and Civil Engineering, China University of Petroleum (East China), Qingdao, China*

[3]*POWERCHINA Huadong Engineering Corporation Limited, Zhejiang, China*

Abstract: Suction caissons are commonly used as foundations for deep-sea offshore wind turbines. However, spudcan penetration from jack-up installation vessels can disturb nearby caissons. Model tests were conducted to investigate the effect of the spudcan penetration on the displacement, rotation, and earth pressure distribution of the adjacent suction caisson in sand. Results show that the motion behavior of the suction caisson during spudcan penetration is a combination of rotational and translational movements. The variations of lateral displacement, vertical displacement and rotation angle of the suction caisson decreases with increasing distance between the spudcan and the caisson. When the spudcan penetration depth equals 0.6 times of the diameter of the spudcan maximum cross-section, the position of the rotation center changes sharply from under the caisson lid to the above the caisson lid, meanwhile from a position away from the spudcan to one close to the spudcan. The peak value of earth pressure increases successively along the suction caisson wall with increasing spudcan penetration depth, which introduces changes in the motion behavior of the suction caisson. In addition, based on the test results, a theoretical method is proposed for predicting the suction caisson rotation angle under spudcan penetration.

Keywords: Offshore wind turbine, Jack-up wind turbine installation vessel, Spudcan penetration, Suction caisson

1. INTRODUCTION

Offshore wind power has been developed worldwide in recent years due to the stable wind energy resources, high power generation efficiency and no occupation of land resources. The total offshore wind power installed capacity in China has remained the highest in the world for four consecutive years. By the end of June 2025, the cumulative grid-connected installed capacity of China offshore wind power reached 44.2 GW, with an additional 2.49 GW of offshore installations added in the first half of 2025 (National Energy Administration, 2025). In December 2024, the largest floating offshore wind turbine in China began operation. With a single-unit installed capacity of 16.6 MW and an installation water depth exceeding 45 meters, it is expected to generate 54 million kWh of clean electricity annually, marking the gradual expansion of China offshore wind power construction into deeper waters (YangJiang Government Network, 2024).

Offshore wind turbine foundations are critical to the safe operation of offshore wind turbines. The most widely used form of offshore wind turbine foundation at present is the large-diameter steel pile. However, the installation of the steel foundation requires huge pile-driving equipment, which leads to a long construction period and high construction costs. The suction caisson is a large-diameter, thin-walled cylindrical structure. The suction caisson is installed to a specific depth first under the self-weight or with ballast. Then a pump is connected and the water inside the suction caisson is pumped out. This creates a negative pressure within the suction caisson, allowing it to be installed to the desired depth under the applied suction. Compared with the pile foundations, the greatest advantage of the suction caisson is that its installation only requires a pump, without the need for huge pile-driving equipment. In addition, the suction caisson is suitable for wide water depths. Currently, the suction caisson has been successfully applied in waters with a depth of over 2000 m. It means that the suction caisson is the optimal choice for deep-sea wind turbine foundations (Newlin *et al*., 2003).

Figure **1** shows the installation procedure of the offshore turbine, after the suction caisson installation, a jack-up wind-turbine installation vessel was usually required to assemble the wind turbine tower, hub, and blades. In addition, the maintenance and replacement of large components of wind turbines requires the use of a jack-up platform. After installation and maintenance operations are completed, the spudcan is pulled out from the seabed and the platform departs from the construction site. A hole is left in the seabed, *i.e*., the footprint.

The spudcan of the jack-up wind-turbine installation vessel must penetrate the seabed to ensure stability, which introduces significant disturbance to the surrounding sand and, consequently, affects the

*Address correspondence to this author at the School of Civil and Architectural Engineering, Shandong University of Science and Technology, Qingdao, China; E-mail: 15905482596@163.com

Received on 09-11-2025 Accepted on 20-12-2025 Published on 26-12-2025

E-ISSN: 000-000/25

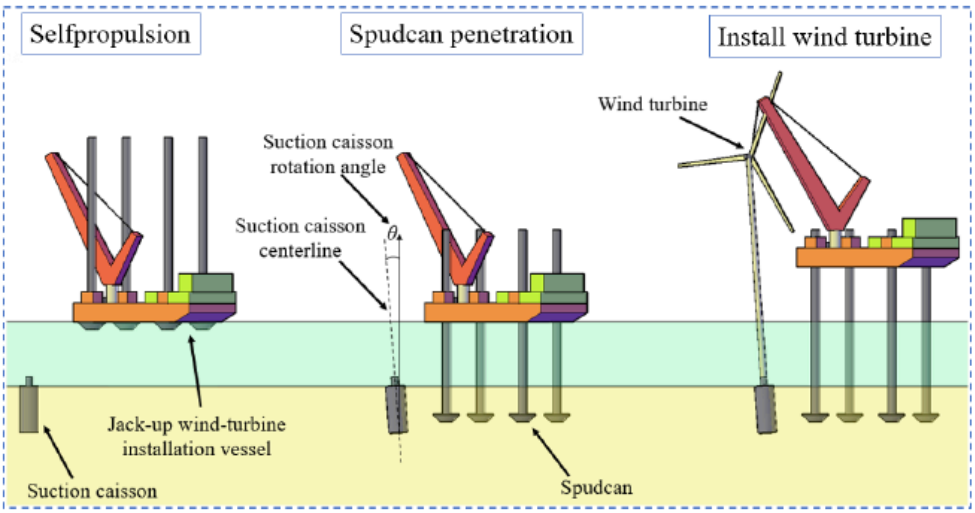

Figure 1: Offshore wind turbine installation process.

performance of the adjacent suction caissons (Li *et al*., 2023; Zhang *et al*., 2025). For example, the large deformation of sand induced by the spudcan penetration can cause the translation and rotation of the suction caisson. The DNV code specifies that the maximum allowable deflection angle of the suction caisson during construction is 0.25°(DNV 2017). Therefore, it is necessary to conduct research on the motion behavior of the suction caisson under the effect of spudcan penetration.

Le *et al*. (2024) found that the rotation angle, peak vertical displacement, and stress on the caisson wall decrease with increasing distance between the spudcan and the caisson. In addition, the stress on the near caisson wall is greater than that on the far caisson wall. Ouyang *et al*. (2024) investigated the response of an adjacent suction-bucket jacket foundation under spudcan penetration and found that the effect is minimized when the angle between the spudcan and the suction caisson is 60°. Based on the numerical simulation results, a theoretical method is proposed for predicting the rotation angle of three-caisson jacket foundations. This method is not applicable to mono-caisson. Li *et al*. (2024) carried out numerical simulations to study the effect of square-spudcan penetration on an adjacent suction caisson in clay, confirmed that the caissons rotate during the spudcan penetration, then an empirical formula to predict the rotation angle was proposed. When the distance between the spudcan and the adjacent suction caisson exceeds 2.0 times of spudcan diameter, the penetration effect can be neglected. However, the motion behavior of the suction caisson under spudcan penetration in sand needs further study.

Besides, both the suction caisson and the cylinder-shaped foundation are thin-walled cylindrical steel tubes, and buckling will occur under the large lateral earth pressure introduced by spudcan penetration. Some studies have been carried out to explore the buckling behavior of the cylinder-shaped foundation (*e.g*., the large-diameter thin-walled steel cylinder as the protective structure of submarine production system) during spudcan penetration. Li *et al*. (2022, 2024) determined that the stress and strain in the foundation wall increase with increasing spudcan penetration depth, and there is a risk of buckling in the wall. However, both the displacement and the stress in the wall decrease exponentially as the distance between the spudcan and the cylindrical foundation increases.

The motion behavior of the suction caisson relies on the flow mechanism of the surrounding sand during spudcan penetration. We can borrow some ideas from conventional piles. Xie *et al*. (2009, 2017) conducted model and centrifuge tests to investigate the interaction mechanism between piles and the surrounding sand during spudcan penetration. Results show that pile displacement is strongly correlated with sand flow, the pile displacement decrease with the decrease of the lateral flow of sand. Additionally, the direction of the pile bending moment reverses from pointing toward the spudcan to pointing away from it as the spudcan penetration depth increases.

Based on the cavity expansion theory and the nonlinear beam model tests, Zhang *et al*. (2021) have put forward a method for predicting the additional bending moment and displacement of adjacent pile during spudcan penetration. This method can be used to determine the critical sections of the piles. Fan *et al*. (2020, 2024) conducted centrifuge model tests and coupled Eulerian–Lagrangian numerical simulations to investigate the effect of spudcan penetration on adjacent piles. Results show that, when the distance between the spudcan and the piles exceeds 1.0 times of the spudcan diameter, the effect of spudcan

penetration decreases with increasing shear strength of the sand. Li *et al*. (2023) point out that as the penetration depth of the spudcan increases, the flow mechanism of the sand around the spudcan changes from local flow to complete flow, and the bending moment of the adjacent piles first increases and then decreases. The effect of the spudcan penetration on the bending moment of the pile group is less significant than that on the mono-pile. When the distance between the spudcan and the pile group exceeds 1.0 *D*s (where *D*s is the spudcan diameter), spudcan penetration has no effect on the bending moment of the adjacent pile group (Yang *et al*., 2020). Wen *et al*. (2023), using the modified Poulos method, conclude that the load-sharing ratio between the near and far pile heads change with increasing spudcan penetration depth. This is because the near pile restricts the lateral flow of the soil, leading to an increase in the bending moment on the near piles and a decrease in the bending moment on the far piles. However, when used the suction caisson as foundation for offshore wind turbines, which is differ significantly from piles in terms of geometry, aspect ratio, and load-transfer mechanisms, the effect of the spudcan penetration on the interaction between the adjacent suction caisson and surrounding sand should be further investigated.

In this study, a series of model tests were conducted in sand to investigate the effects of spudcan penetration on the motion behavior of the adjacent suction caissons. The novelty and key contributions are as follows: (i) The lateral displacement, vertical displacement, and rotation angle of adjacent suction caissons were investigated under various spudcan-caisson spacings and penetration depths;(ii) The minimum safe spudcan-caisson spacing and critical spudcan penetration depth to ensure the safe operation of the adjacent suction caisson were obtained; (iii) The earth pressure distribution around the suction caisson during spudcan penetrating into sand was clarified, and the relationship between sand flow mechanism and the suction caisson motion behavior was established; (iv) Method for predicting suction caisson rotation angle during spudcan penetration was proposed. This study is aimed at providing theoretical guidance for the practical engineering of offshore wind turbine construction.

2. MODEL TESTS

2.1. Test Equipment

2.1.1. Spudcan and Suction Caisson Models

The spudcan and suction caisson models (as shown in Figures **2** and **3**) were scaled down from the

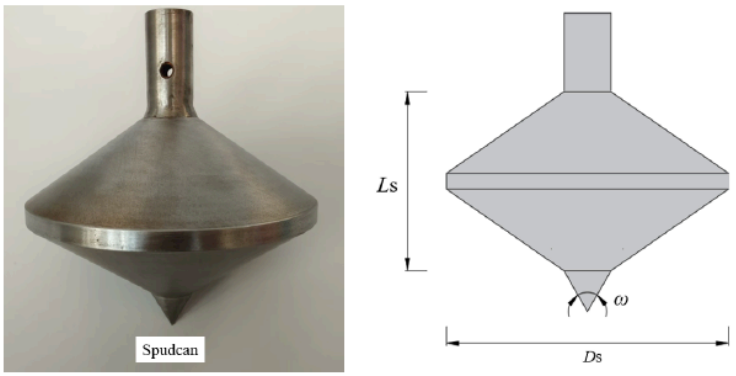

Figure 2: Spudcan model.

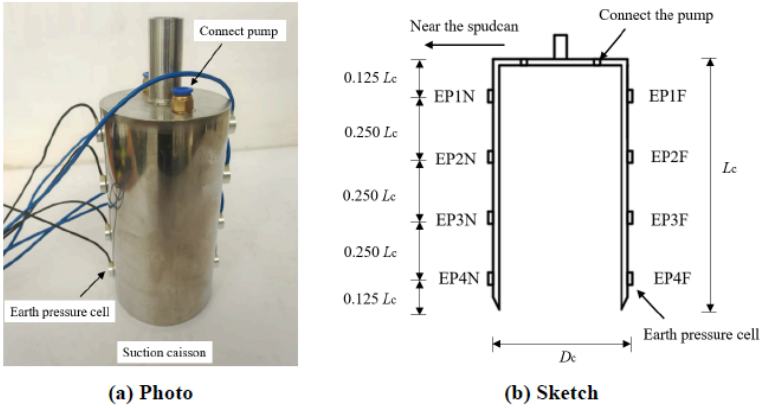

Figure 3: Suction caisson model.

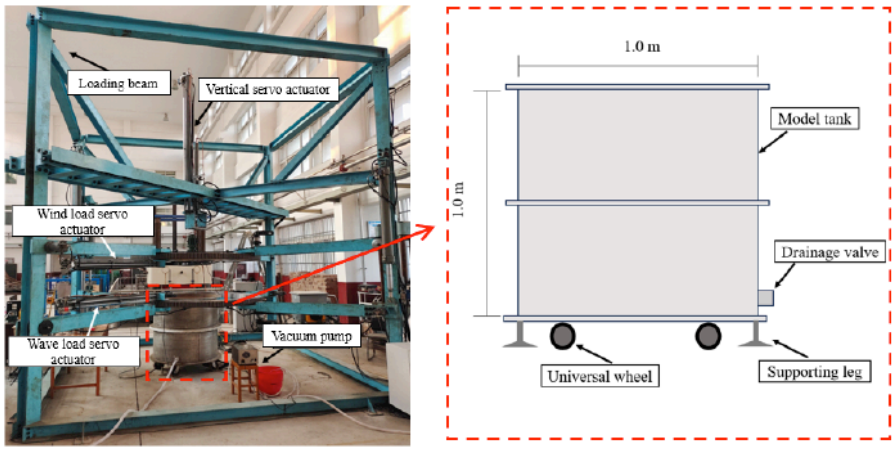

Figure 4: Combine loading system.

prototype at a ratio of 1:50. The spudcan is a solid steel spindle-shaped foundation with a diameter (D_s) of 200 mm, a height (L_s) of 114 mm, and a conical tip angle of 60°. A loading rod is mounted at the center of the top of the spudcan, which is connected to a vertical servo actuator. The diameter (D_c) of the suction caisson model is 100 mm, the height (L_c) is 200 mm, and both the thickness of the caisson lid (t_1) and the thickness of the caisson wall (t_2) are 2 mm. It is assumed that during spudcan penetrating sand, the deformations of the suction caisson wall and lid are very small and can be neglected. Therefore, the suction caisson is regarded as rigid. In addition, the model tank diameter and height are all equal to 1.0 m. The deformation range of the sand around the suction caisson under the lateral ultimate load is approximately 2.2 D_c. When the distance between the model tank wall and the suction caisson wall is greater than 3 D_c, the effect of the boundary effect can be eliminated (Li *et al*. 2014).

2.1.2. Loading System and Model Tank

As shown in Figure **4**, the spudcan is penetrated by using vertical servo actuator. The vertical servo actuators are divided into the primary servo actuator and the auxiliary servo actuator. The primary servo actuator can bear a load of 40 kN and is used for positioning the rods and for the penetration of the foundation. The auxiliary servo actuator can bear a load of 0.3 kN and is used to apply low vertical loads and cyclic loads to the already installed foundation. In this experiment, the main servo actuator was used to penetrate the spudcan.

The model tank is a steel cylindrical container. The bottom of the model tank is equipped with four universal wheels, which can adjust the position of the model tank. After adjusting the model tank to the appropriate position, it is fixed by the supporting legs to prevent the model tank from moving during the test. There is a drainage valves located at the model tank bottom dissipating water during sand consolidation.

2.1.3. Sand Used

The test sand was collected from the Yellow Sea in China. Figure **5** shows the particle size distribution curve of the sand, which indicates that it is poorly graded. The parameters of the sand are given in Table **1**. The thickness of sand is 6 L_s, which can eliminate the boundary effect during the spudcan penetration. During the sand layer preparation, sand was scattered evenly into the tank filled with water. Then, the drainage valve at the base of the model tank was kept open to improve consolidation efficiency during the sand consolidation.

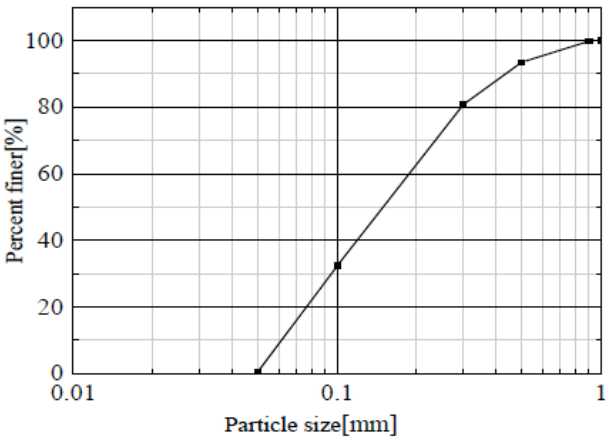

Figure 5: Sand particle size distribution curves.

Table 1: Parameters of Sand

γ'/(kN/m3)	C_u	C_c	D_{50}(mm)	D_r	e_{max}	e_{min}	k（cm/s）	φ
9.5	3.083	0.865	0.167	0.667	0.935	0.628	0.002	28°

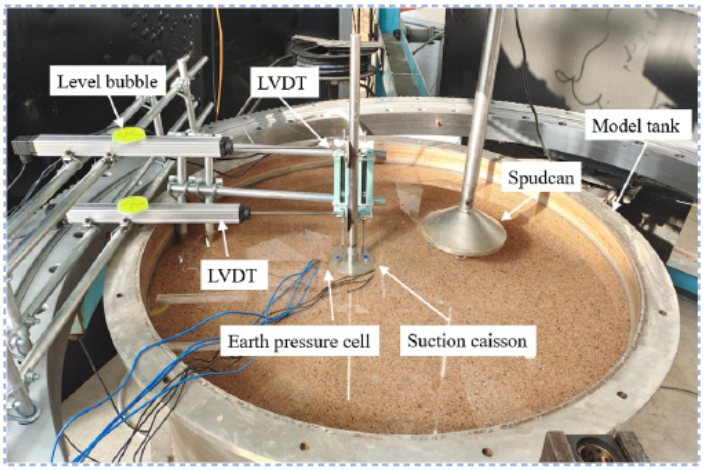

Figure 6: Test set-up.

2.1.4. Measuring Equipment

As shown in Figure **6**, to measure the lateral displacement of the suction caisson, two lateral displacement transducers were arranged along the loading rod of the suction caisson. The distances between the measurement points y_1 and y_2 were offset upward from the suction caisson lid by 1.0 D_c and 2.5 D_c respectively. Two vertical displacement transducers were arranged on each side of the suction caisson, close to and away from the spudcan. The distance between the vertical displacement transducers and the suction caisson centerline were 0.2 D_c.

In addition, to measure the earth pressure around the suction caisson during spudcan penetration, eight earth pressure cells were installed on each side of the suction caisson wall, both close to and away from the spudcan. The depths of the earth pressure cells were 0.125 L_c, 0.375 L_c, 0.625 L_c, and 0.875 L_c (shown in Figure **3** (**b**)).

2.2. Test Procedures

2.2.1. Spudcan Penetration Test

To investigate the effect of boundary effects on the spudcan penetration, the level bubble method (Zhang *et al*. 2024) was used to measure the deformation range of the surrounding sand caused by the penetration of the spudcan (as shown in Figure **7**). When the spudcan penetrates the sand bed, the deformation of the surrounding sand is symmetrical (Ding *et al*. 2022). Five rows of level bubbles are evenly distributed in the 1/4 sector around the spudcan. The diameter of each bubble is 6 mm and the length is 15

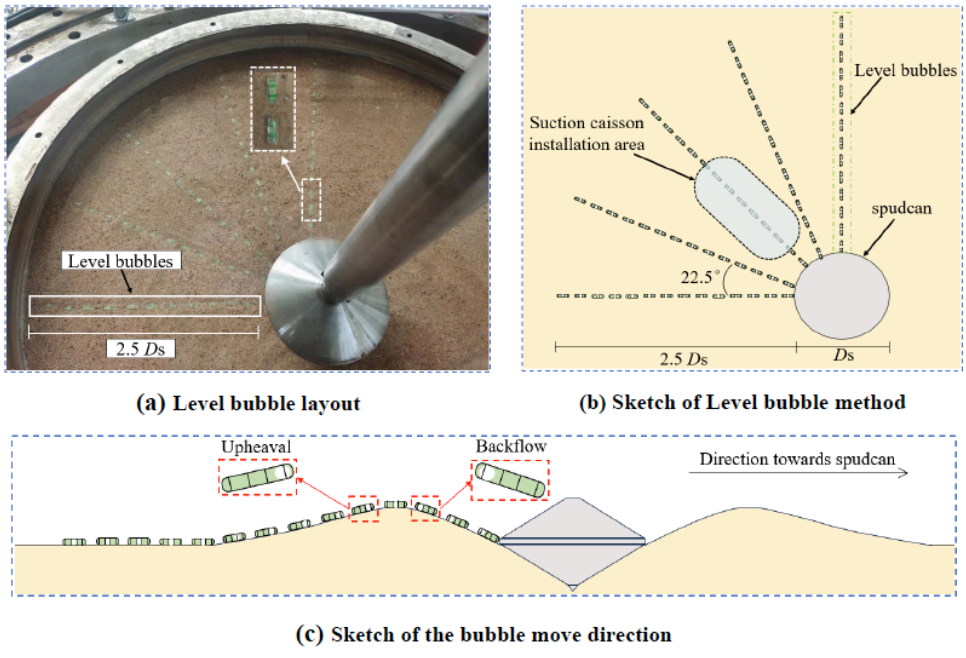

Figure 7: The level bubble method measuring the deformation of sand surface.

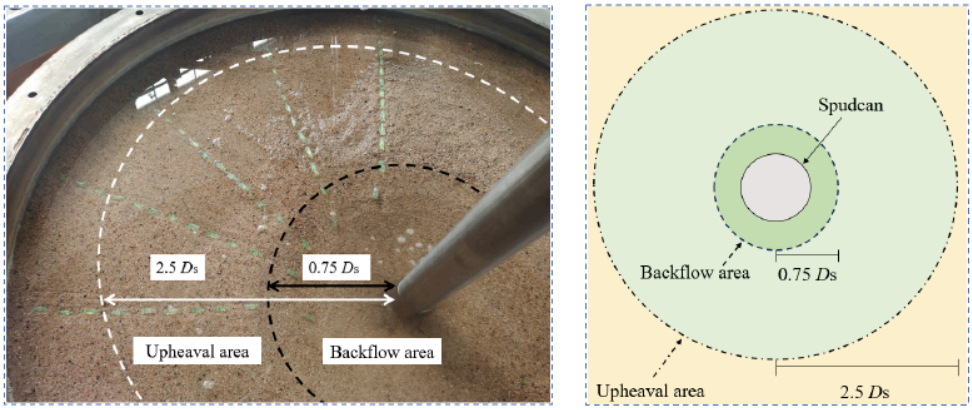

(a) Sand deformation photo **(b) Sand deformation fitted curve**

Figure 8: Sand deformation around the spudcan.

mm. The distance between adjacent bubbles in each row is 10 mm. The angle between adjacent rows of level bubbles is 22.5°. Each row of level bubbles extends 2.5 D_s outward from the edge of the spudcan.

As can be seen from Figure **8**, the deformation range of the sand around the spudcan is a positive circle extending outward from the spudcan centerline with a radius of 2.5 D_s. Within the 0.75 D_s range around the spudcan, the level bubbles are buried in the sand as the sand backflow. In addition, the installation area of the suction caisson is given in Figure **7**(**b**). The minimum distance between the suction caisson wall and the spudcan edge is 0.5 D_s, and the peak distance is 1.0 D_s. Within the installation area of the suction caisson, the sand deformation direction caused by the penetration of the spudcan is relatively uniform. It can be considered that the penetration of the spudcan is not affected by the boundary of the model tank. The penetration of the spudcan has a reliable effect on the test results of the motion behavior mode of the adjacent suction caisson.

The required bearing capacity of the spudcan model is 4.8 kN, scaled from the prototype. The bearing capacity of the spudcan in sand can be calculated using the method from the SNAME code.The penetration resistance when the maximum cross-section of the spudcan above the soil surface can be obtained by Eq. (1):

$$F_{v1} = \left(0.5\gamma' B N_\gamma s_\gamma d_\gamma + p_0' N_q s_q d_q\right) A \tag{1}$$

where, γ' is the effective unit weight of the sand, kN/m^3; N_γ=(1.5N_q-1)tanφ; B is the maximum diameter of the spudcan, m; S_γ=0.6; d_γ=1; N_q=e$^{\pi\tan\varphi}$tan^2(45+φ/2); p_0' is the effective stress at the deepest point of the largest diameter of the spudcan; S_q=1+ tanφ; d_q=1+2P tanφ(1-sinφ)/D; P is the spudcan penetration depth, m; A is the maximum cross-sectional area of the spudcan, m^2.

When the penetration depth of the spudcan maximum cross-section below the sand surface, the surrounding sand flow back into the cavity. Therefore, the penetration resistance of the spudcan can be calculated using the Eq.(2) for the condition of complete soil backflow.

$$F_v = F_{v1} - F_0' A + \gamma' V \tag{2}$$

where, F_0' is the effective additional pressure generated on the bearing surface of the spudcan due to the overlying soil, kPa; V is the volume of the spudcan, m^3.

The resistance of the spudcan increases linearly with increasing penetration depth (as shown in Figure **9**). The model test results show good agreement with the theoretical results. At a penetration depth of 0.3 D_s, the resistance meets the bearing capacity requirements. However, we want to investigate the response of the suction caisson when the maximum section of the spudcan exceeds the suction caisson tip. Therefore, the final spudcan penetration depth is set to 1.0 D_s.

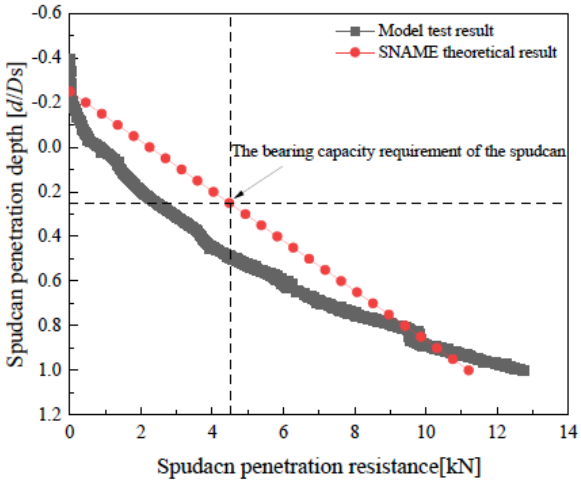

Figure 9: Validation of the spudcan penetration resistance.

(a) Determination of suction caisson position (b) Excavation of suction caisson pit

Figure 10: Suction caisson installation using pre-embedded method.

2.2.2. Motion Behavior of the Suction Caisson under the Spudcan Penetration

The suction caisson models were installed using the pre-embedded installation method and the suction-assisted installation method. For the suction caisson installed by pre-embedded method, the sand needed to be filled inside the suction caisson and compacted, then the suction caisson was installed in desired area (as shown in Figure **10**). After the suction caisson installation, the model tank is filled with water through the bottom valve from the bottom up, ensuring complete saturation of the sand soil. The water surface was kept 10 cm high above the mud surface. Then the drainage valve at the bottom of the model tank was kept open until the water level decreased to 2 cm high above the sand surface, allowing for sand consolidation.

For the suction caisson installed by suction -assisted installation method, the air and water inside the suction caisson were pumped out at a pumping rate of 200 mL/min assisting the suction caisson to desired depth. The sand consolidation time for both pre-embedded installation and suction -assisted installation is 20 minutes. The spudcan was penetrated after the installation of the suction caisson was completed, with a penetration speed of 0.15 mm/s and a penetration depth of 1 D_s. The test cases are shown in Table **2**.

3. TEST RESULTS

As shown in Figure **11**, the initial stage of the spudcan penetration is that the conical tip of the spudcan is in contact with the sand surface. However,

Table 2: Testing Programs

Installation Method	Penetration Depth of Spudcan d/D_s	Distance between Caisson and Spudcan l/D_s
Suction installation	0.3,0.6,1.0	0.5,0.75,1.0
Pre-embedded installation		

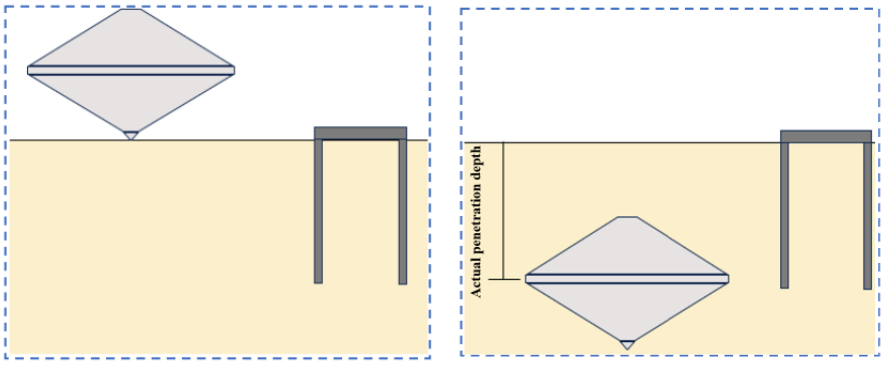

(a) Initial stage (a) Final stage

Figure 11: Initial stage and final stage of spudcan penetration.

the actual penetration depth is determined by the depth of the largest cross-section of the spudcan. Therefore, the dimensionless penetration depth value is negative during the initial stage of spudcan penetration. When the spudcan reaches its peak penetration depth, the depth of its largest cross-section is the same as the depth of the suction caisson tip.

The results of the model tests can be applied to the actual engineering of the prototype, through dimensionless processing (Kelly *et al*. 2006). The penetration depth of the spudcan (*d*)is dimensionless as d/D_s. The distance between the spudan and the suction caisson (*l*)is dimensionless as l/D_s. The lateral displacement (*h*) and vertical displacement (*v*) of the suction caisson are dimensionless as h/D_c and v/D_c respectively. The rotation angle of the suction caisson is in radian form. In addition, the earth pressure of the suction caisson wall (*P*) is dimensionless as $P/D_c\gamma'$.

3.1. Suction Caisson Displacement during Spudcan Penetration

3.1.1. Lateral Displacement of Suction Caisson

Figure **12** illustrates the behavior of the lateral displacement of the suction caisson during the spudcan penetration. The distance between the measurement point and the suction caisson lid is 2.5 D_c. The positive direction of the suction caisson lateral displacement is defined as the suction caisson moving away from the spudcan, and the negative when moving towards the spudcan.

The lateral displacement behavior of the suction caisson installed by the pre-embedded method and the suction-assist method are significantly different. With increasing spudcan penetration depth, the lateral displacement of the pre-embedded suction caisson first increases in the positive direction and then increases in the negative direction. However, the lateral displacement of the suction caisson using the suction-assist method increases in a single direction with increasing spudcan penetration depth.

When the distance between the spudcan and the suction caisson is less than 0.75 D_s, the lateral displacement of the suction caisson using suction-assist installation increases in the negative direction. When the distance between the spudcan and the suction caisson is equal to 1.0 D_s, the behavior of the lateral displacement of the suction caisson installed by suction-assist and the pre-embedded suction caisson is the same. As the depth of the spudcan penetration increases, the lateral displacement of the suction caisson installed by suction-assist first increases in the positive direction and then gradually stabilizes. This indicates that when the distance between the spudcan and the suction caisson is greater than or equal to 1.0 D_s, the installation method only impacts the lateral displacement of the suction caisson and has a relatively small effect on the motion behavior of the suction caisson.

The effect of the spudcan penetration on the displacement of the suction caisson was evaluated by the lateral displacement variation. It should be noted that for the suction caisson installed using the suction-assist method, the variation of the displacement equals the final displacement, which can be calculated by Eq. (3):

$$\Delta h = (h_p - h_e)/D_c \tag{3}$$

where, h_p is the peak value of the suction caisson lateral displacement; h_e is the final value of the suction caisson lateral displacement; Δh is the lateral displacement variation of suction caisson.

The lateral displacement variation decreases with increasing distance between the spudcan and the suction caisson, indicating that the effect of the spudcan penetration on the adjacent suction caisson decreases. In addition, the lateral displacement variation of the suction caisson installed by the suction-assist method is always less than that of the suction caisson installed by the pre-embedded method. When the distance between the spudcan and the suction caisson equals 0.5 D_s, 0.75 D_s, and 1.00 D_s, the lateral displacement variation of the suction caisson installed by the pre-embedded method is 0.130 D_c, 0.057 D_c, and 0.018 D_c, while the lateral displacement variation of the suction caisson installed by the suction-assist method is 0.066 D_c, 0.024 D_c, and 0.001 D_c, respectively.

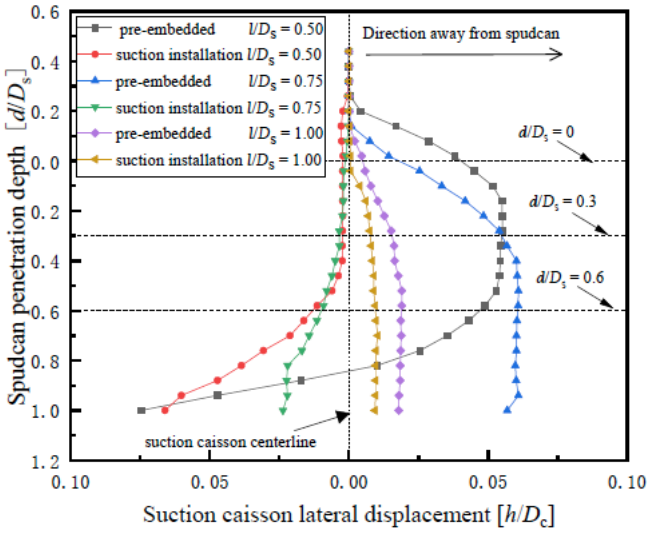

Figure 12: Lateral displacement of suction caisson during spudcan penetration under varying distances.

3.1.2. Vertical Displacement of Suction Caisson

Figure **13** shows the behavior of the suction caisson vertical displacement during the spudcan penetration. The measurement point for vertical displacement is located on the side of the suction caisson away from the spudcan. The behavior of the vertical displacement of the suction caisson installed by suction-assist method is the same as that of the suction caisson installed by pre-embedded method. The upward lifting direction of the suction caisson is defined as the positive direction of the vertical displacement. With increasing penetration depth of the spudcan, the vertical displacement of the suction caisson increases along the negative direction until the maximum cross-section of the spudcan reaches the sand surface, and then the vertical displacement increases along the positive direction approximately linearly. The variation of the vertical displacement of the suction caisson can be obtained through Eq. (4):

$$\Delta v = (v_p - v_e)/D_c \tag{4}$$

where, v_p is the peak value of the suction caisson vertical displacement; v_e is the final value of the suction caisson vertical displacement; Δv is the vertical displacement variation of suction caisson.

The vertical displacement variation of suction caisson decreases with increasing the distance between the spudcan and the suction caisson. The vertical displacement variation of the suction caisson installed by the suction-assist method is always less than that of the suction caisson installed by the pre-embedded method. When the distance between the spudcan and the suction caisson equals 0.5 D_s, 0.75 D_s, and 1.00 D_s, the vertical displacement variation of the suction caisson installed by the pre-embedded method is 0.253 D_c, 0.174 D_c, and 0.081 D_c, while the vertical displacement variation of the suction caisson installed by the suction-assist method is 0.238 D_c, 0.139 D_c, and 0.052 D_c, respectively. Indicating that the results of the suction caisson installed by the pre-embedded method are more conservative than those of the suction caisson installed by the suction-assist method.

When the suction caisson is installed using the suction-assist method, seepage occurs from outside to inside the suction caisson along the suction caisson wall. This results in an increase in the relative density of the sand outside the suction caisson wall, while the relative density inside the suction caisson decreases (as shown in Figure **14**). The lower relative density inside the suction caisson reduces the friction between the suction caisson wall and the sand, leading to increased settlement and decreased upheaval values for the suction caisson.

In practical engineering, the suction caisson is installed by using the suction-assist method. In this study, the earth pressure cell is first affixed to the outer wall of the suction caisson before conducting the test. This process can significantly disturb the surrounding sand during the suction-assisted installation and subsequent penetration of the spudcan. To mitigate the impact of the earth pressure cell on the test results, the suction caisson is installed using a pre-embedded method. The lateral and vertical displacements variation of suction caissons installed using the suction-assist method are always less than those using the pre-embedded method. Therefore, using the pre-embedded method to predict the displacement of adjacent suction caissons under spudcan penetration provides a higher safety margin.

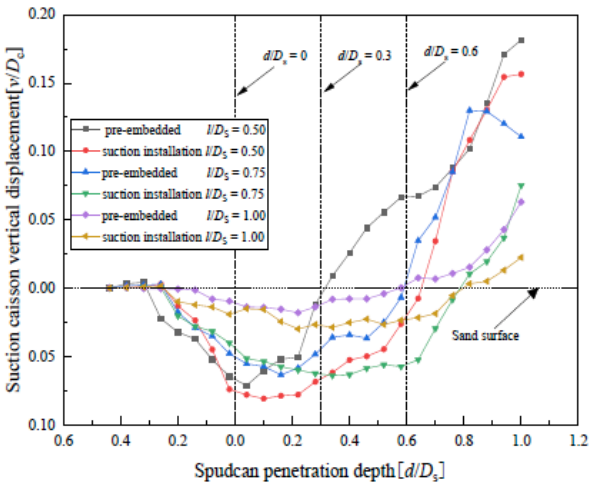

Figure 13: Vertical displacement of suction caisson during spudcan penetration under varying distances.

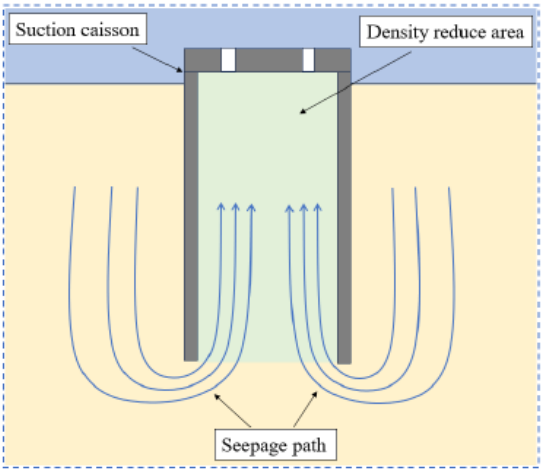

Figure 14: Sketch of seepage path under the applied suction.

3.2 Rotation Behavior of the Suction Caisson During Spudcan Penetration

3.2.1 Rotation Angle of the Suction Caisson

Figure **15** shows the calculation sketch of the rotation angle. The rotation angle can be calculated

using the displacement of two measurement points, as given by Eq. (5):

$$tan\theta = \frac{x_1 - x_2}{y_1 - y_2} \tag{5}$$

where, θ is the rotation angle of the suction caisson; y_1 and y_2 are the distances between the two measurement points and the suction caisson lid; x_1 and x_2 are the lateral displacements of the two measurement points.

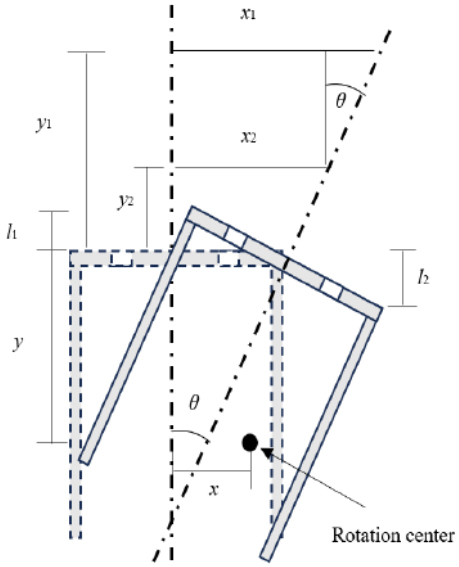

Figure 15: Diagram of the calculation of the rotation center of the suction caisson.

The development direction of the rotation center of the suction caisson changes with increasing spudcan penetration depth. The positive direction of the suction caisson rotation angle is defined as the suction caisson moving away from the spudcan, and the negative direction when the suction caisson moving towards the spudcan. With an increase in the spudcan penetration depth, the rotation angle increases to a peak value in the positive direction and then turns to the negative direction. In addition, the peak value of the suction caisson rotation angle occurs later as the distance between the suction caisson and the spudcan increases. Therefore, the Eq. (6) is used to calculated the variation of the suction caisson rotation angle:

$$\Delta\theta = \theta_p - \theta_e \tag{6}$$

where, θ_p is the peak value of the suction caisson rotation angle; θ_e is the final value of the suction caisson rotation angle; $\Delta\theta$ is the rotation angle variation of suction caisson.

When the distance between the spudcan and the suction caisson equals 0.5 D_s, 0.75 D_s, and 1.00 D_s, the rotation angle variation of suction caisson are 0.0016 rad, 0.0005 rad, and 0.00026 rad, respectively. The rotation angle variation of the suction caisson decreases with increasing distance between the suction caisson and the spudcan, indicating that the stability of the suction caisson increases with increasing distance between the suction caisson and the spudcan (as shown in Figure **17**).

Besides, the final rotation angle of the suction caisson decreases with an increase in the spudcan penetration depth. When the distance between the spudcan and the suction caisson equals 0.5 D_s, 0.75 D_s, and 1.00 D_s, the final rotation angles of the suction caisson are -0.0014 rad, 0.0003 rad, and -0.00016 rad, respectively. This indicates that the final rotation angle of the suction caisson at various distances between the suction caisson and the spudcan is less than 0.0043 rad.

The DNV code specifies that the maximum rotation angle of the suction caisson during installation must be less than 0.25°. Therefore, it is necessary to develop a theoretical method for predicting the rotation angle of the suction caisson under the influence of spudcan penetration. As can be seen in Section 3.3.1, the rotation angle of the suction caisson (θ) is affected simultaneously the distance between the spudcan and the suction caisson (l/D_s) and the spudcan penetration depth (d/D_s). To simplify the calculation, the rotation angle of the suction caisson is first fitted under various spudcan penetration depths based on the test results. The relationship between the suction caisson rotation angle and the spudcan penetration depth can be obtained using the Eq. (7):

$$\begin{cases} \frac{\theta\pi}{180} = 0.00014 + 0.00046\left(\frac{d}{D_s}\right) - 0.00022\left(\frac{d}{D_s}\right)^2 - 0.00173\left(\frac{d}{D_s}\right)^3, \left(\frac{l}{D_s} = 0.5\right) \\ \frac{\theta\pi}{180} = 0.000083 + 0.00045\left(\frac{d}{D_s}\right) - 0.00016\left(\frac{d}{D_s}\right)^2 - 0.001\left(\frac{d}{D_s}\right)^3, \left(\frac{l}{D_s} = 0.75\right) \\ \frac{\theta\pi}{180} = 0.000024 + 0.00021\left(\frac{d}{D_s}\right) - 0.00018\left(\frac{d}{D_s}\right)^2 - 0.0006\left(\frac{d}{D_s}\right)^3, \left(\frac{l}{D_s} = 1.0\right) \end{cases} \tag{7}$$

Based on the model test results, the relationship between the suction caisson rotation angle and the spudcan penetration depth is described by cubic polynomial functions. The rotational angle of the suction caisson under any l/D_s can be expressed by Eq. 8:

$$\frac{\theta\pi}{180} = f_1 + f_2\left(\frac{d}{D_s}\right) - f_3\left(\frac{d}{D_s}\right)^2 - f_4\left(\frac{d}{D_s}\right)^3 \tag{8}$$

where, f_1, f_2, f_3 and f_4 are the are the fitted coefficients. As shown in Figure **16**, the fitted coefficients are related to the l/D_s.

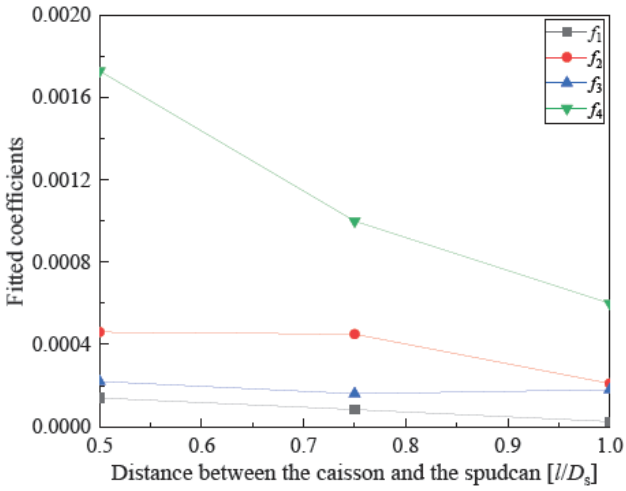

Figure 16: Relationship between the coefficients and the distance between the caisson and the spudcan.

Therefore, the relationship between the fitted coefficients and l/D_s can be fitted using Eq. (9):

$$\begin{cases} f_1 = 0.00026 - 0.00023\left(\dfrac{l}{D_s}\right) \\ f_2 = 0.00021 - 0.00224\left(\dfrac{l}{D_s}\right) + 0.00182\left(\dfrac{l}{D_s}\right)^2 \\ f_3 = 0.00056 - 0.001\left(\dfrac{l}{D_s}\right) + 0.00061\left(\dfrac{l}{D_s}\right)^2 \\ f_4 = 0.00414 - 0.00616\left(\dfrac{l}{D_s}\right) + 0.00261\left(\dfrac{l}{D_s}\right)^2 \end{cases} \quad (9)$$

The fitted coefficients f_1, f_2, f_3 and f_4 under a certain distance between the suction caisson and the spudcan are calculated using Eq. (9), and then substituted into Eq. (8). The suction caisson rotation angle under the combined effect of the spudcan penetration depth and the distance between the suction caisson and the spudcan can be obtained.

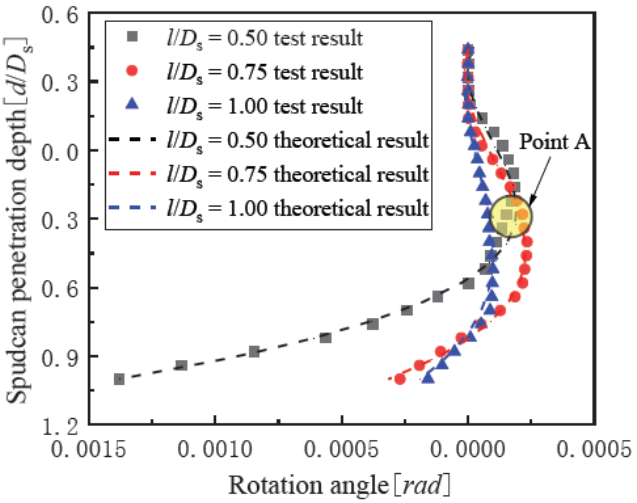

Figure 17: Comparison of the theoretical results and experimental results of the rotation angle.

Figure **17** presents the theoretical results of the suction caisson rotation angle under the effect of the spudcan penetration. The maximum difference between the theoretical results and the test results occurs at l/D_s =0.5 D_s, d/D_s=0.3 D_s (point A in Figure **17**). At this point, the theoretical results have increased by 23% compared to the test results. Due to the sand backflow into the hole above the spudcan, the unloading of sand around the suction caisson close to the spudcan is significant (as shown in Figure **18**). This leads to the suction caisson rotation angle decreasing sharply compared to that predicted by the theoretical method. Indicating that when the distance between the spudcan and suction caisson is less than 0.5 D_s, the risk of suction caisson overturning instability increases. Therefore, the distance between suction caisson and spudcan should be greater than 0.5 D_s.

However, this prediction formula is exclusively based on model test results and does not take into account the impact of the physical and mechanical properties of the sand on the rotation angle of the suction caisson. Additionally, it fails to consider factors such as sand strain softening and backflow. In the model tests, the rotation angle of the suction caisson is determined by the relative position between the spudcan and the suction caisson. Further numerical simulations will be carried out across a wide range of conditions to explore how key parameters-including sand relative density, friction angle, dilation angle, effective unit weight, and the geometric characteristics of both the spudcan and suction caisson—affect the rotation angle of the suction caisson.

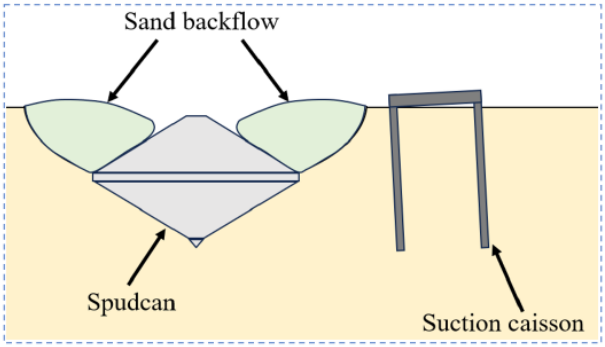

Figure 18: Diagram of sand backflow around the suction caisson.

The functions discussed in this article are fitting functions that characterize the relationship between the rotation angle of the suction caisson and the penetration of the spudcan. However, the limited sample size poses a risk of overfitting. There are many factors influence of the adjacent suction caisson rotation angle during spudcan penetration. To enhance the analysis efficiency and achieve the optimal prediction of the rotation angle of the suction caisson under the influence of multiple factors and the spudcan

penetration. Further study will be conducted investigating extensive parameter studies through model tests, numerical simulations, and machine learning. The test results in this article can provide training and validation data for machine learning.

3.2.2 Behavior of the Suction Caisson Rotation Center

The distance between the rotation center and the suction caisson lid and the distance between the rotation center and the suction caisson centerline can be obtained by using the Eqs. (10) and (11):

$$y = \frac{x_1 y_2 - x_2 y_1}{x_2 - x_1} \tag{10}$$

$$x = d_x \frac{l_1 - l_2}{l_1 + l_2} \tag{11}$$

Where, y is the distance between the rotation center and the suction caisson lid (when y is less than 0, it indicates that the rotation center is lower than the suction caisson lid); x is the distance between the rotation center and the suction caisson centerline (when x is less than 0, it indicates that the rotation center is close to the spudcan); dx is the distance between the vertical measurement point and the suction caisson centerline. l_1 and l_2 are the vertical displacements close to and away from the spudcan, respectively.

Figure **19** shows the distance between the rotation center and the caisson lid, with the yellow area representing the internal area of the suction caisson. The behavior of the rotation center position is the same at various distances between the spudcan and the suction caisson. When the spudcan penetration depth is less than 0.6 D_s, the distance between the rotation center and the suction caisson lid first increases and then decreases, reaching final stability. When the spudcan penetration depth reaches 0.6 D_s, the position of the rotation center changes sharply from below the suction caisson lid to above the caisson lid, and then moves towards the caisson lid. In addition, with increasing the distance between the spudcan and the suction caisson, the rotation center moves downwards. The variation of the rotation center position decreases with increasing the distance between the spudcan and the suction caisson. When the distance between the spudcan and the suction caisson equals 0.5 D_s, 0.75 D_s, and 1.00 D_s, the variation of the vertical rotation center position change are 22.81 D_c, 17.9 D_c, and 12.2 D_c respectively.

Figure **20** shows the distance between the rotation center and the caisson centerline, with the yellow area representing the internal area of the suction caisson. When the spudcan penetration depth reaches 0.3 D_s, the rotation center moves across the suction caisson centerline from a position close to the spudcan to one away from the spudcan. However, when the spudcan penetration depth reaches 0.6 D_s, the position of the rotation center changes sharply from a position away from the spudcan to one close to the spudcan. Furthermore, the lateral variation of the rotation center increases with increasing the distance between the spudcan and the suction caisson. When the distance between the spudcan and the suction caisson equals 0.5 D_s, 0.75 D_s, and 1.00 D_s, the variation of the lateral rotation center position change are 0.31 D_c, 0.80 D_c, and 1.50 D_c respectively.

When the rotation center of the suction caisson is located outside the caisson, its motion behavior is a combination of translation and rotation, with translation being the dominant factor. As shown in Figures **19** and **20**, the rotation center is always located outside the suction caisson during spudcan penetration, indicating that translation is the dominant component of its motion.

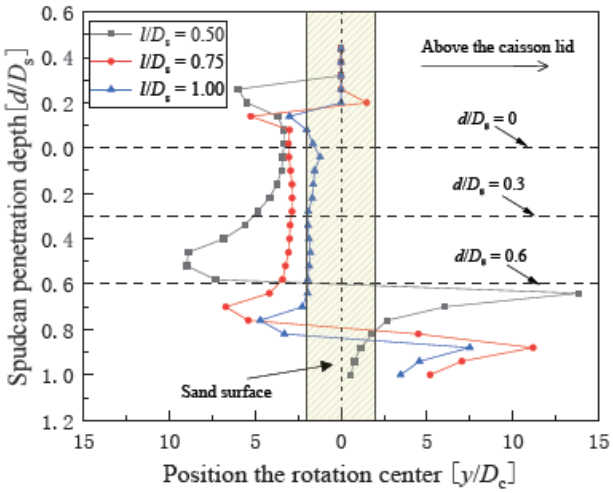

Figure 19: The distance between the rotation center and the caisson lid.

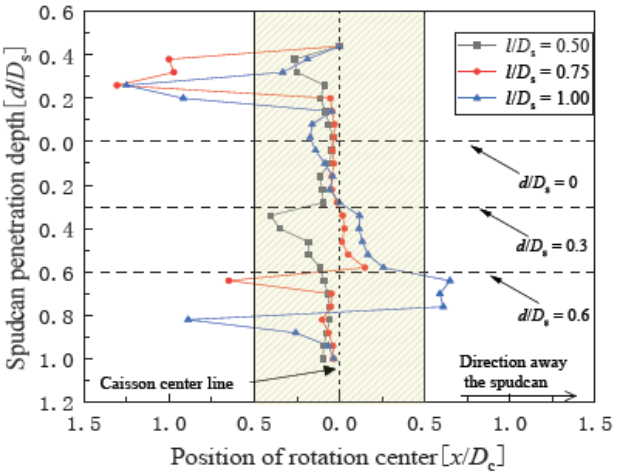

Figure 20: The distance between the rotation center and the caisson centerline.

3.3. Interaction Between the Suction Caisson and Surrounding Sand

The additional stress induced in the surrounding sand by spudcan penetration leads to rotation and lateral displacement of the adjacent suction caisson. Therefore, it is necessary to investigate the relationship between the sand flow mechanism and the motion behavior of the suction caisson.

3.3.1. Distribution of the Earth Pressure Around the Suction Caisson

Figure **21** illustrates that the relationship between the earth pressure around the suction caisson and the spudcan penetration depth. By adding the earth pressure on the front side and the rear side, the total earth pressure acting on the suction caisson is obtained. As the spudcan penetration depth increases, the earth pressure at each measurement point initially increases and then decreases, with the peak values of the earth pressure at each measurement point occur successively. When the spudcan penetration depth exceeds the depth of the earth pressure measurement point, the sand above the maximum cross-section of the spudcan begins to unload, resulting in a decrease in the earth pressure surrounding the suction caisson.

In addition, the peak value of the earth pressure at each measurement points increase with increasing spudcan penetration depth. The peak value of the earth pressure at the measurement point at 0.875 D_s reaches the maximum value. Buckling will occur when the suction caisson wall is subjected to large lateral stress. However, due to the relative stiffness of the model test being greater than that of the prototype, no buckling occurred on the suction caisson wall during spudcan penetration. When designing the suction caisson in actual engineering, it is necessary to verify whether the lateral additional stress induced by spudcan penetration on the suction caisson wall exceeds the design allowable value.

In addition, the maximum value of the earth pressure around the suction caisson decreases with an increase in the distance between the spudcan and the suction caisson. When the distance between the spudcan and the suction caisson equals 0.5 D_s, 0.75 D_s, and 1.00 D_s, the dimensionless maximum earth pressure are 6.07, 3.52, and 2.85.

3.3.2. Relationship Between Sand Flow and Motion Behavior of Suction Caisson

Figure **22** gives the earth pressure distribution along the suction caisson wall under the spudcan penetration. The distribution of the earth pressure changes gradually with increasing spudcan penetration depth. When the spudcan penetration depth is less than 0.3 D_s, the maximum earth pressure occurs at the measurement points of 0.125 D_s and 0.375 D_s, while the minimum earth pressure occurs at the measurement points of 0.625 D_s and 0.875 D_s. However, when the spudcan penetration depth exceeds 0.6 D_s, the maximum earth pressure occurs at the measurement points of 0.625 D_s and 0.875 D_s, while the minimum earth pressure occurs at the measurement points of 0.125 D_s and 0.375 D_s. This indicates that the position where the maximum sand lateral flow volume occurs moves downward with increasing spudcan penetration depth, and the sand backflow area always occurs above the maximum cross-section of the spudcan.

Analyze in conjunction with the variation behavior of the suction caisson rotation angle in Section 3.2. When the spudcan penetration depth is less than 0.3 D_s, the maximum earth pressure induced by the sand lateral flow concentrates on the upper part of the suction caisson, leading to the suction caisson rotation and displacement in the direction away from the spudcan. When the spudcan penetration depth is between 0.3 D_s and 0.6 D_s, the position of the maximum earth pressure moves downward along the suction caisson wall, and the rotation center is outside the suction caisson

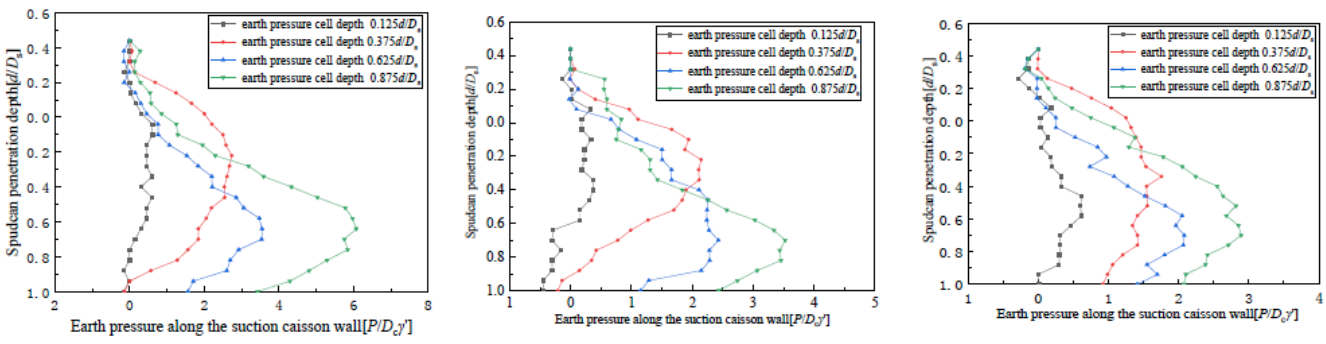

（a） 0.5 *Ds* （b） 0.75 *Ds* （c） 1 *Ds*

Figure 21: Relationship between the earth pressure and the penetration depth of the spudcan under various distance between spudcan and the suction caisson.

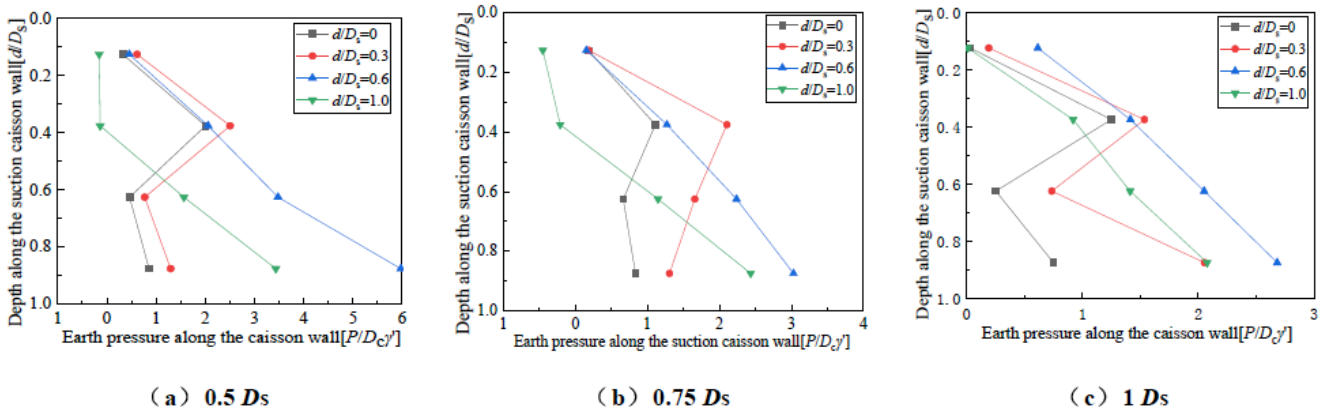

（a） 0.5 *D*s （b） 0.75 *D*s （c） 1 *D*s

Figure 22: The earth pressure distribution along the suction caisson wall under the spudcan penetration.

(Figure **18**). Therefore, the rotation of the suction caisson can be ignored, and the motion behavior is primarily translational. When the spudcan penetration depth exceeds 0.6 D_s, the maximum earth pressure concentrates on the lower part of the suction caisson. Meanwhile, the sand above the maximum cross-section of the spudcan unloads due to sand backflow. As a result, the suction caisson rotates and displaces in the direction toward the spudcan.

Furthermore, the earth pressure along the suction caisson decreases when the spudcan penetration depth reaches 1.0 D_s compared to 0.6 D_s. This indicates that the maximum earth pressure occurs under the maximum cross-section of the spudcan. When the spudcan penetration depth is 1.0 D_s, the sand above the cross-section of the spudcan has experienced varying degrees of load reduction. The degree of unloading decreases with increasing distance between the spudcan and the suction caisson. The phenomenon of sand unloading will affect the behavior of the lateral capacity, which will be investigated in the future.

4. CONCLUSIONS

Model tests were conducted to investigate the motion behavior of suction caisson induced by the penetration of spudcan in sand. The conclusions are as follows:

(1) The variation of the lateral displacement and the vertical displacement decrease with increasing distance between the spudcan and the suction caisson. Minimum operational distance of 1.0 *D*s should be maintained between spudcan and adjacent suction caisson during jack-up vessel operations.

(2) The motion behavior of the suction caisson is dominated by translational motion. When the spudcan penetration depth reaches 0.6 times the spudcan diameter, the position of the rotation center changes sharply. Provided that the foundation bearing capacity is sufficient, the spudcan penetration depth should be less than 0.6 times the spudcan diameter.

(3) The peak earth pressure around the suction caisson at the 0.875 D_s measurement point reaches the maximum value. In practical engineering, it is necessary to verify the maximum earth pressure on the suction caisson wall to prevent caisson wall buckling.

(4) Based on the test results, a theoretical method for predicting the rotation angle of the suction caisson in sand is proposed. Before construction, the suction caisson rotation angle for the specified spudcan penetration depth and spudcan-caisson spacing should be calculated using the theoretical method.

CREDIT AUTHORSHIP CONTRIBUTION STATEMENT

Yukun Zhang: Supervision, Investigation, Writing – original draft. Dayong Li: Supervision, Methodology, Project administration, Funding acquisition, Writing - editing. Qian Xiang: Data curation, Validation, Writing - editing. Senjie Tong: Formal analysis.

DECLARATION OF COMPETING INTEREST

The authors declare that they have no known competing financial interests or personal relationships that could have appeared to influence the work reported in this paper.

DATA AVAILABILITY

Data will be made available on request.

ACKNOWLEDGEMENTS

This research is supported by the Natural Science Foundation of China (Grant Nos. 52471289, 52371301).

REFERENCES

[1] Ding, K., Fan, S., Dong, S.. Multilayer-perceptron-based prediction of sand-over-clay bearing capacity during spudcan penetration. International Journal of Naval Architecture and Ocean Engineering. 2022; 14: 100479. https://doi.org/10.1016/j.ijnaoe.2022.100479

[2] DNV (Det Norske Veritas). DNVGL-RP-C212 offshore sand mechanics and geotechnical engineering. Bærum, Norway: DNV. 2017.

[3] Fan, Y. F., Wang, J. H.. Method to Evaluate Effect of Spudcan Penetration on Adjacent Jacket Piles. Applied Ocean Research. 2020; 106: 102436. https://doi.org/10.1016/j.apor.2020.102436

[4] Fan Y. F., Guo D, and Cheng X. L. *et al*. A modified soil reaction model for laterally-loaded piles considering the effects of spudcan penetration. Ocean Engineering. 2024; 309: 118355. https://doi.org/10.1016/j.oceaneng.2024.118355

[5] Kelly R B, Byrne B W, Houlsby G T. A comparison of field and laboratory tests of caisson foundations in sand and clay. Géotechnique, 2006; 56(9): 617-626. https://doi.org/10.1680/geot.2006.56.9.617

[6] Le, C.H., Hu H., Wang X. Study on Influence of Spudcan Penetration Pile on adjacent Bucket Foundation In Sandy Sand, Acta Energiae Solaris Sinica. 2024; 45(02): 95-101. (in Chinese)

[7] Li D. Y., Feng, L. Y., and Zhang, Y. K. *et al*. Model tests of modified suction caissons in marine sand under monotonic lateral combined loading. Applied Ocean Research, 2014; 48: 137-147. https://doi.org/10.1016/j.apor.2014.08.005

[8] Li, C. F., Zhang, H. Y., Liu R., *et al*. Research on the Influence of Spudcan Penetration and Extraction on Adjacent Platform Piles in Sand. International Journal of Geomechanics. 2023; 23(7): 04023083. https://doi.org/10.1061/IJGNAI.GMENG-8100

[9] Li, S. Y., Qi, Y. L., Zhou, M., *et al*. Response of an Installed Suction Caisson Induced by Rectangular Footing Penetration in Nonhomogeneous Clay. International Journal of Geomechanics. 2024; 24(9): 04024195. https://doi.org/10.1061/IJGNAI.GMENG-9368

[10] Li, S. Z., Shen, X. P., Chen, B. M., *et al*. Influence of spudcan penetration on the stability of adjacent steel cylinder in sand. Ships and Offshore Structures. 2022; 18: 1-10. https://doi.org/10.1080/17445302.2022.2062159

[11] Li, S. Z., Cao, M. T., and Shen, X. P., *et al*. Centrifugal model tests on effects of spudcan penetration on adjacent steel cylinder in clay, Chinese Journal of Geotechnical Engineering. 2024; 46(S1): 152-157. (in Chinese)

[12] Li, X. B., Liu, J., and Wang, X. Z., *et al*. Bending moment response of batter piles in clay under spudcan-pile interaction. Applied Ocean Research. 2023; 138: 103670. https://doi.org/10.1016/j.apor.2023.103670

[13] National Energy Administration. Text transcript of the National Energy Administration press conference in the third quarter of 2025. https://www.nea.gov.cn/20250731/83ffa46373ec42dd99e0e3271028c151/c.html#,(Accessed 17 September 2025).

[14] Newlin, J. A.. Suction anchor piles for the Na Kika FDS mooring system Part 2: Installation performance. Deepwater Mooring Systems Concepts, Design, Analysis, and Materials, Houston, TX: ASCE, 2003; 55-75. https://doi.org/10.1061/40701(2003)4

[15] Ouyang Q. J., Qi Y. L., and Zhou M., *et al*. Optimization of Spudcan Penetration and Influence on Caisson Foundation. Applied Ocean Research, 2024; 152: 104186. https://doi.org/10.1016/j.apor.2024.104186

[16] SNAME, Recommended Practice for Site Specific Assessment of Mobile Jack-Up Units, Rev3, America, The Society of Naval Architects and Marine Engineers. 2008.

[17] Wen, C. Q., Wang, J. H., Yan, X. W. Analysis for Model Test of Pile Cluster Effect Influenced by Spudcan Footings Penetration, Port Engineering Technology. 2023; 60(01): 33-37+52. (in Chinese)

[18] Xie, Y. I.. Centrifuge model study on Spudcan-pile interaction. Ph D, National University of Singapore. 2009.

[19] Xie, Y., Leung, C. F., Chow, Y. K.. Centrifuge modelling of spudcan–pile interaction in soft clay overlying sand. Géotechnique. 2017; 67(1): 1-9. https://doi.org/10.1680/jgeot.15.P.031

[20] Yang, X. T., Wang, J. H., Fan Y.F.. Model tests on effects of spudcan penetration on an adjacent pile group. Hydro-Science and Engineering. 2020; (3): 75-81. (in Chinese)

[21] Yangjiang government network. The world's largest floating wind power platform, "Mingyang Tiancheng", has been put into operation. 2024. http://www.yangjiang.gov.cn/gnlm/sylbt/content/post_828474.html, (Accessed 17 September 2025). https://doi.org/10.3390/su17177679

[22] Zhang, H. Y., Liu, R., Jia, Z. L.. Investigation of effect of spudcan penetration on adjacent platform piles, Chinese Journal of Geotechnical Engineering. 2021; 43(05):867-876. (in Chinese)

[23] Zhang Y. K., Xiang, Q., and Li, D. Y., *et al*. Sand deformation behavior around modified suction caissons during lateral loading and analytical method obtaining lateral bearing capacity. Ocean Engineering. 2024; 300: 117367. https://doi.org/10.1016/j.oceaneng.2024.117367

[24] Zhang, Y. K., Zheng, H., and Li D. Y., *et al*. Influence of spudcan penetration and extraction on motion behavior and lateral bearing capacity of adjacent suction caisson. Rock and Sand Mechanics. 2025; 46(8): 2325-2338. (in Chinese)

© 2025 Zhang *et al.*
This is an open-access article licensed under the terms of the Creative Commons Attribution License (http://creativecommons.org/licenses/by/4.0/), which permits unrestricted use, distribution, and reproduction in any medium, provided the work is properly cited.